

# Progress towards two-dimensional biomedical imaging with THz spectroscopy

Matthew C Beard, Gordon M Turner and Charles A Schmuttenmaer

Department of Chemistry, Yale University, 225 Prospect Street, PO Box 208107, New Haven, CT 06520-8107, USA

Received 5 March 2002

Published 17 October 2002

Online at [stacks.iop.org/PMB/47/3841](http://stacks.iop.org/PMB/47/3841)

## Abstract

Terahertz spectroscopy represents a frontier in the field of biomedical imaging. It is possible to image complex objects that are opaque to visible and infrared light. In this paper, we have used THz imaging to reveal the structure inside a sunflower seed. We compare images based on time- and frequency-domain representations of the THz scans, and conclude that for this type of specimen the time-domain THz scans provide more detailed information than their frequency-domain counterparts.

## 1. Introduction and background

Imaging capabilities are of fundamental importance in medicine and biology. Ever since Wilhelm Roentgen produced the striking x-ray image of Professor von Kolliker's hand, including his ring, during a public lecture on 23 January 1896 [1], the medical community has been acutely aware of the tremendous possibilities afforded by the ability to visualize or capture an image that cannot be observed with the naked eye. Examples include optical microscopy, x-rays, ultrasound, positron emission tomography (PET), computer-aided tomography (CAT), magnetic resonance imaging (MRI), fluorescence microscopy, multiphoton-induced fluorescence microscopy, infrared imaging and Raman imaging. Each of these techniques has unique capabilities and limitations. X-rays, ultrasound, PET, CAT and MRI are of particular interest because they are non-invasive and images can be obtained *in vivo*. The various microscopies find more use in the field of pathology.

This paper is concerned with performance of a time-domain terahertz (THz) spectrometer capable of two-dimensional (2D) imaging. Electromagnetic waves at THz frequencies fall between the microwave and infrared regions of the spectrum. This region is often referred to as the far-infrared (FIR). It is largely unexplored mainly due to lack of bright sources. THz time-domain spectroscopy (THz-TDS) employs a method of coherent detection that allows a pulsed THz source to be used even though the average power is below the level of blackbody radiation. This technique can be used to image fatty tissue, bone, teeth and thin slices of non-fatty tissue. One of its unique aspects is that the time-dependent electromagnetic waveform is measured



**Figure 1.** Photograph of the sunflower seed imaged using 2D THz spectroscopy. The dots indicate the locations of the scans shown in figure 2.

at each spatial location. This allows both the frequency-dependent absorption coefficient and frequency-dependent refractive index to be measured simultaneously over a frequency range from 0.2 THz to 4 THz on a grid with  $\sim 400 \mu\text{m}$  spatial resolution or better. Consequently, a great deal of spatial and spectral information about the sample is collected. Instruments based on THz spectrometers will complement existing biomedical imaging technologies.

THz imaging of plant and animal material was first reported in 1995 [2, 3]. In this context, THz spectroscopy is often referred to as T-ray imaging [4, 5]. It has been possible to image biological samples, with especially striking results of specimens that have a high contrast of aqueous and non-aqueous regions. THz tomography is still in its infancy, but the initial work done by Nuss and Mittleman, [6] and more recent studies [4, 7] have shown that there is great potential. For example, the various layers comprising a computer floppy disk were revealed by deconvolving the input THz waveform from the reflected waveform [4]. The development of tomographic techniques will be absolutely essential for the use of THz imaging in biological media, especially when absorption by water within the sample limits the applicability of THz transmission studies.

In this paper, we present a THz 2D imaging study of a sunflower seed obtained in transmission mode. This object was chosen because it is composed of two different types of material, the shell and the kernel, and has features on a relatively small length scale. It is shown that both the attenuation and delay of the THz pulse provide valuable information about the object being imaged.

## 2. Experimental details

The spectrometer used for THz time-domain spectroscopy (THz-TDS) has been described in detail previously [8–10]. Note, these are not time-resolved measurements; the name merely implies that the measurements are made in the time-domain, and then Fourier transformed into the frequency domain. The design of this spectrometer is based on descriptions in [11] and [12], and is a standard configuration. The THz waveform is mapped out by incrementally stepping an optical delay line that controls the moment at which the propagating electric field is instantaneously sampled. One of the significant advantages of THz-TDS is that the sign of the field is determined in addition to its magnitude. The THz waveform transmitted through the sample is collected as the sample is raster-scanned through the beam waist, and a 2D image is built up. Full information of the frequency-dependent absorption coefficient and refractive index in the FIR is obtained at each point sampled.

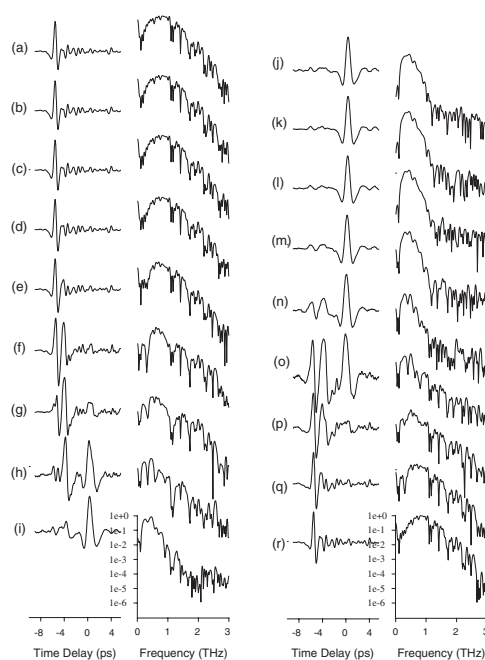


**Figure 2.** The time- and frequency-domain spectra obtained for the representative cut shown in figure 1. The scans (a)–(r) correspond to the highest dot to the lowest. The time-domain scans have been normalized, and are plotted with a linear vertical scale. The frequency-domain power spectra are plotted with a logarithmic vertical scale as indicated for scans (i) and (r). The plots have been offset vertically for clarity.

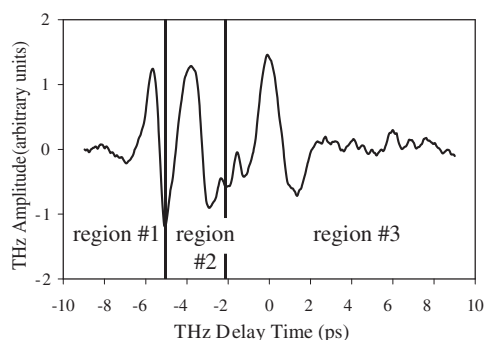


**Figure 3.** Scan showing peaks due to pulse travelling around the entire seed (region no 1), travelling through the shell but not kernel (region no 2) and through both the shell and kernel (region no 3). This is an enlarged view of scan (o) in figure 2.

### 3. Results and discussion

Figure 1 shows a photograph of a sunflower seed with a vertical line of dots indicating the spatial locations at which the series of THz scans shown in figure 2 were taken. The transmitted time-domain THz waveform may exhibit peaks in three different temporal regions, as illustrated in a representative scan shown in figure 3. The entire image of the seed shown in figure 4 was obtained by collecting THz scans at each point of a 2D grid at uniform intervals of  $625 \mu\text{m}$ . The overall image size is 15 mm horizontally  $\times$  10.625 mm vertically (18 rows  $\times$  25 columns). Each scan requires 30 s to collect, leading to 225 min for the image which

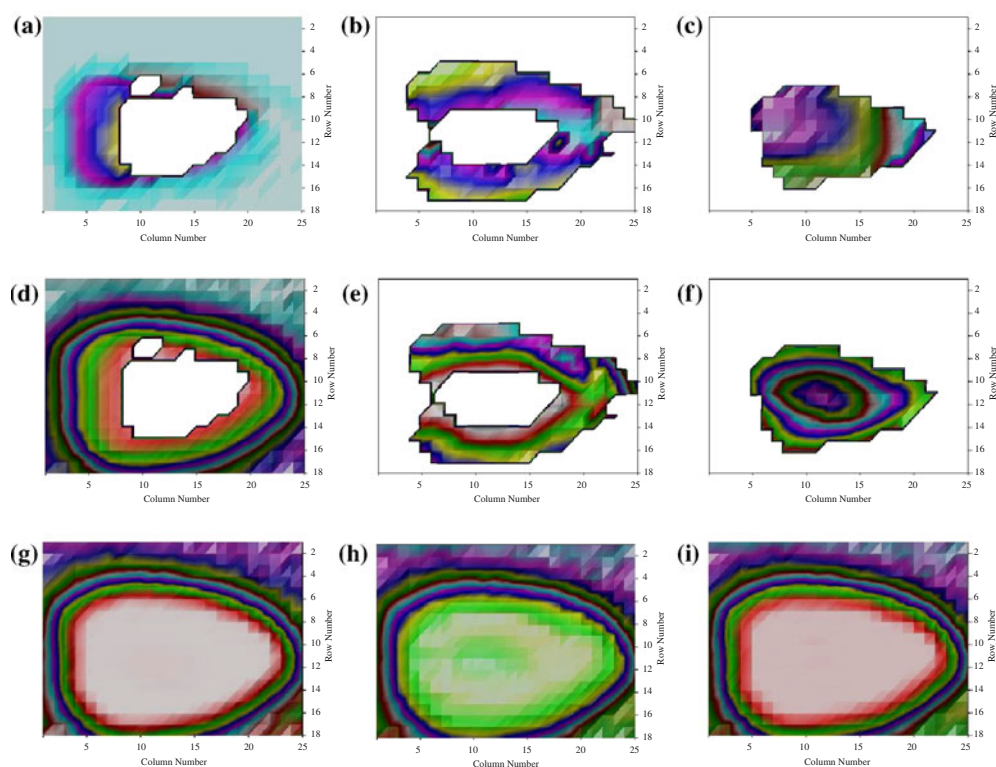


**Figure 4.** Top row: 2D maps corresponding to arrival time of peaks numbers 1, 2 and 3. Middle row: 2D maps corresponding to the height of peaks numbers 1, 2 and 3. Bottom row: 2D maps of total power, peak frequency and mean frequency based on frequency-domain data. In all nine plots, the colour scale is arbitrary and is simply employed to highlight the variations.

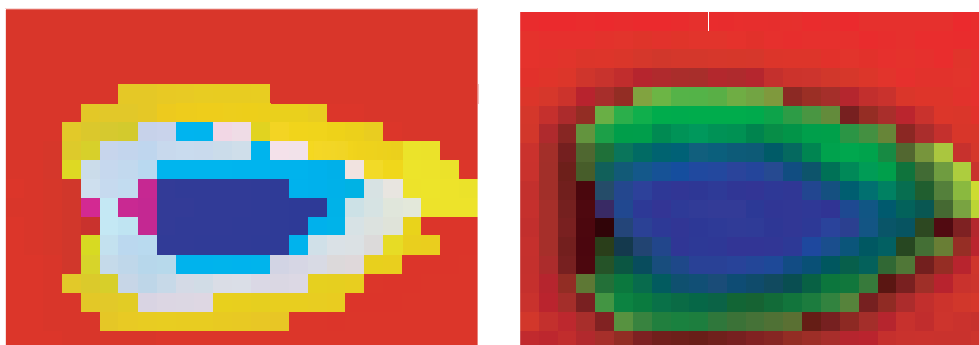


**Figure 5.** False colour images generated by letting information about peaks numbers 1, 2 and 3 dictate the amount of red, green and blue, respectively. Left: using peak arrival times (based on the top row of figure 4). Right: using peak heights (based on middle row of figure 4). Once again, the shell/kernel structure is evident.

contains 450 points. The scanning speed is primarily limited by the relatively slow optical delay line employed, and the amount of time required to move the sample from one point to another. Other workers have demonstrated significantly faster data acquisition rates, allowing a scan to be taken in roughly 20 to 100 ms [3, 13, 14]. Thus, the time for the entire image would be reduced to 10–50 s.



**Figure 6.** Photograph of sunflower seed used in THz imaging experiment after opening it to reveal the internal structure.

There is a peak in region number 1 (seen in figures 2(a)–(e) and (q)–(r)) when the pulse does not pass through the seed at all, and therefore is not delayed. There will be a peak in region number 2 (figures 2(f)–(h) and (o)–(p)) when the pulse traverses the shell surrounding the kernel, but not the kernel itself. Finally, there will be a peak in region number 3 (figures 2(h)–(o)) when the pulse travels through both the shell and kernel. The frequency-domain representation is obtained by Fourier transforming each of the time-domain scans and is shown to the right of the time-domain scans in figure 2. The sharp absorption features in the power spectra are due to absorption by water vapour and can be eliminated by purging the beam path with dry  $N_2$ . There is significant attenuation of the high frequency components of the pulse when it travels through the kernel. This is manifested in the time-domain scans as a broadening of the THz pulse, and in the frequency-domain as a loss of power at frequencies above  $\sim 1$  THz.

Two-dimensional maps characterizing the arrival times and peak heights within the three regions, as well as frequency-domain data, are shown in figure 4. The arrival time of the peak in region numbers 1, 2 and 3 are shown in (a), (b) and (c), respectively. The arrival time is indicative of how much material the pulse has travelled through. The peak heights in region numbers 1 to 3 are shown in (d)–(f), respectively, and are also sensitive to the amount of material the pulse passes through. Finally, figure 4 displays 2D maps of quantities obtained from the frequency-domain data. The peak frequency, mean frequency, and integrated intensity are shown in (g), (h) and (i), respectively. Each row of figure 4 (peak arrival time, peak height or frequency-domain data) exhibits subtle nuances unique to the quantity being plotted, but the structure inside the seed is most clearly revealed in the time-domain images. For example, the quasi-annular region corresponding to the pulse travelling through the shell but not the kernel is easily identified in (b) and (e) of figure 4, whereas this region is not obvious in the panels based on frequency-domain representations of the data ((g)–(i)).

Since there are three peaks of interest in the time-domain scans, one can make a false-colour image by combining the 2D maps for peak height or arrival time. Let peak number 1 correspond to the red intensity, peak number 2 correspond to green and peak number 3 correspond to blue. These false-colour images for peak arrival time and peak height are shown in figure 5. For comparison, a photograph of the opened seed is shown in figure 6. The ability of THz imaging to uncover the details of the internal structure of the seed is evident.

#### 4. Conclusions

There has been work reported in the literature describing 2D THz imaging [3, 4, 7, 13, 15–23], and 3D imaging to a lesser extent [6, 24–30]. Two-dimensional *biomedical* THz imaging is becoming increasingly important. One of the most significant characteristics of this new technique is that the measurements are made in the time-domain, and both the pulse arrival time and amplitude provide valuable information. Were this not the case, this type of experiment

could be carried out on a standard Fourier transform FIR spectrometer fitted with a pair of focusing mirrors around the sample. We have shown that by being able to divide the scan into regions, and measuring the peak height and arrival time within each region, reveals a detailed picture of the sample under study.

## References

- [1] Bleich A R 1960 *The Story of X-Rays* (New York: Dover)
- [2] Lipkin R 1995 T rays for two *Sci. News* **148** 136–7
- [3] Hu B B and Nuss M C 1995 Imaging with terahertz waves *Opt. Lett.* **20** 1716–8
- [4] Hunsche S, Mittleman D M, Koch M and Nuss M C 1998 New dimensions in T-ray imaging *IEICE Trans. Electron.* **81** 269–76
- [5] Mickan S, Abbott D, Munch J, Zhang X C and van Doorn T 2000 Analysis of system trade-offs for terahertz imaging *Microelectron. J.* **31** 503–14
- [6] Mittleman D M, Hunsche S, Boivin L and Nuss M C 1997 T-ray tomography *Opt. Lett.* **22** 904–6
- [7] Mittleman D M, Gupta M, Neelamani R, Baraniuk R G, Rudd J V and Koch M 1999 Recent advances in terahertz imaging *Appl. Phys. B* **68** 1085–94
- [8] Kindt J T and Schmuttenmaer C A 1996 Far-infrared dielectric properties of polar liquids probed by femtosecond terahertz pulse spectroscopy *J. Phys. Chem.* **100** 10373–9
- [9] Venables D S and Schmuttenmaer C A 1998 Far-infrared spectra and associated dynamics in acetonitrile-water mixtures measured with femtosecond THz pulse spectroscopy *J. Chem. Phys.* **108** 4935–44
- [10] Beard M C, Turner G M and Schmuttenmaer C A 2000 Transient photoconductivity in GaAs as measured by time-resolved terahertz spectroscopy *Phys. Rev. B* **62** 15764–77
- [11] Smith P R, Auston D H and Nuss M C 1988 Subpicosecond photoconducting dipole antennas *IEEE J. Quantum Electron.* **24** 255–60
- [12] Fattinger C and Grischkowsky D 1989 Terahertz beams *Appl. Phys. Lett.* **54** 490–2
- [13] Jiang Z P and Zhang X C 1998 Single-shot spatiotemporal terahertz field imaging *Opt. Lett.* **23** 1114–6
- [14] Zhao G, Schouten R N, van der Valk N, Wenckebach W T and Planken P C M 2002 Design and performance of a THz emission and detection setup based on a semi-insulating GaAs emitter *Rev. Sci. Instrum.* **73** 1715–9
- [15] Brucherseifer M, Nagel M, Bolivar P H, Kurz H, Bosserhoff A and Buttner R 2000 Label-free probing of the binding state of DNA by time-domain terahertz sensing *Appl. Phys. Lett.* **77** 4049–51
- [16] Brucherseifer M, Bolivar P H, Klingenberg H and Kurz H 2001 Angle-dependent THz tomography-characterization of thin ceramic oxide films for fuel cell applications *Appl. Phys. B* **72** 361–6
- [17] Hunsche S, Koch M, Brener I and Nuss M C 1998 THz near-field imaging *Opt. Commun.* **150** 22–6
- [18] Jiang Z P and Zhang X C 1999 2D measurement and spatio-temporal coupling of few-cycle THz pulses *Opt. Express* **5** 243–8
- [19] Jiang Z P and Zhang X C 1999 Terahertz imaging via electrooptic effect *IEEE Trans. Microw. Theory Tech.* **47** 2644–50
- [20] Mitrofanov O *et al* 2000 Terahertz near-field microscopy based on a collection mode detector *Appl. Phys. Lett.* **77** 3496–8
- [21] Mitrofanov O *et al* 2000 Near-field microscope probe for far infrared time domain measurements *Appl. Phys. Lett.* **77** 591–3
- [22] Mitrofanov O *et al* 2001 Terahertz pulse propagation through small apertures *Appl. Phys. Lett.* **79** 907–9
- [23] Wu Q, Hewitt T D and Zhang X C 1996 Two-dimensional electro-optic imaging of THz beams *Appl. Phys. Lett.* **69** 1026–8
- [24] Cheville R A and Grischkowsky D 1995 Time-domain terahertz impulse ranging studies *Appl. Phys. Lett.* **67** 1960–2
- [25] Cheville R A, McGowan R W and Grischkowsky D R 1997 Late-time target response measured with terahertz impulse ranging *IEEE Trans. Antennas Propag.* **45** 1518–24
- [26] Cheville R A, McGowan R W and Grischkowsky D 1998 Time resolved measurements which isolate the mechanisms responsible for terahertz glory scattering from dielectric spheres *Phys. Rev. Lett.* **80** 269–72
- [27] McClatchey K, Reiten M T and Cheville R A 2001 Time resolved synthetic aperture terahertz impulse imaging *Appl. Phys. Lett.* **79** 4485–7
- [28] Reiten M T, Grischkowsky D and Cheville R A 2001 Properties of surface waves determined via bistatic terahertz impulse ranging *Appl. Phys. Lett.* **78** 1146–8
- [29] Dorney T D, Johnson J L, Van Rudd J, Baraniuk R G, Symes W W and Mittleman D M 2001 Terahertz reflection imaging using Kirchhoff migration *Opt. Lett.* **26** 1513–5
- [30] Johnson J L, Dorney T D and Mittleman D M 2001 Enhanced depth resolution in terahertz imaging using phase-shift interferometry *Appl. Phys. Lett.* **78** 835–7